Planar Millimeter-Wave Antennas: A Comparative Study

Kamil PÍTRA, Zbyněk RAIDA

Dept. of Radio Electronics, Brno University of Technology, Purkyňova 118, 612 00 Brno, Czech Republic

xpitra01@stud.feec.vutbr.cz, raida@feec.vutbr.cz

Abstract. *The paper describes the design and the experimental verification of three types of wideband antennas. Attention is turned to the bow-tie antenna, the Vivaldi antenna and the spiral antenna designed for the operation at millimeter waves. Bandwidth, input impedance, gain, and directivity pattern are the investigated parameters. Antennas are compared considering computer simulations in CST Microwave Studio and measured data.*

Keywords

Vivaldi antenna, bow-tie antenna, spiral antenna, ultra-wideband (UWB) communication, millimeter waves.

1. Introduction

The boom of the ultra-wideband (UWB) technology has increased the demands on small wideband antennas. The Vivaldi antenna (Fig. 1a), the bow-tie antenna (Fig. 1b), the spiral antenna (Fig. 1c) and potential modifications belong among the most published structures [1]–[6].
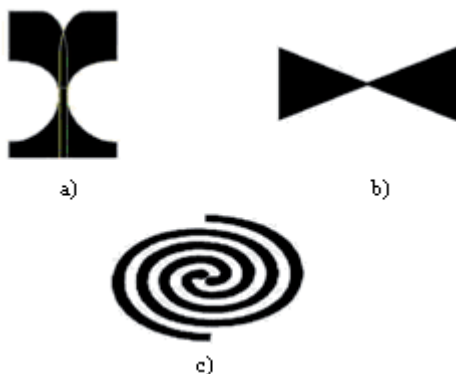

Fig. 1. Examples of wideband antennas: a) Vivaldi antenna, b) bow-tie antenna, c) spiral antenna.

An UWB antenna has to meet the following condition [4]:

$$\frac{B_f}{f_c} > 0.2 .$$ (1)

The bandwidth B_f is determined by the frequencies at which the return loss at the antenna input decreases below -10 dB. The symbol f_c denotes the central frequency of the given frequency band. Moreover, the directivity of the antenna should be constant over the whole frequency band B_f.

In this paper, attention is turned to the design and experimental comparison of three types of wideband antennas: the Vivaldi antenna [1], [5], [7], [6], the bow-tie dipole [1], [2], [7], and the spiral antenna [1], [7]. All the antennas have been simulated in CST Microwave Studio; have been manufactured and measured, and a detailed comparison is presented.

Section 2 of this paper is devoted to the design and measurements of the Vivaldi antenna. The bow-tie antenna is described in section 3, and the spiral antenna is presented in section 4. Section 5 concludes the paper.

2. Vivaldi Antenna

The antenna radiates through an aperture created by a tapered slot between the antenna arms. The investigated antenna was designed for the microwave substrate Arlon 25N (with height $h = 0.788$ mm, permittivity $\varepsilon_r = 3.24$, and loss factor $\tan \delta = 0.0025$ at $f = 10$ GHz).

The description of the design procedure follows:

The lowest operational frequency f_D determines the width of the aperture W_1 and the length of the antenna L (Fig. 2) [6]

$$W_1 = R_{S1} = L = \frac{c}{f_D} \sqrt{\frac{2}{\varepsilon_r + 1}} .$$ (2)

Here, c is the velocity of light, and ε_r denotes the relative permittivity of the substrate.

The arms of the Vivaldi antenna are ellipses with radii R_1 and R_2, R_{s1} and R_{s2} [6]:

$$R_1 = \frac{W_1}{2} + \frac{W_2}{2} ,$$ (3)

$$R_2 = \frac{W_1}{2} - \frac{W_2}{2} ,$$ (4)

$$R_{S1} = W_1 = L, \qquad (5)$$

$$R_{S2} = \frac{R_2}{2}. \qquad (6)$$

In (3) to (6), W_1 denotes the width of the aperture, W_2 denotes the width of the feeding strip (7), and L is the length of the antenna given by (1).

The dimensions of the radiators are chosen so that the distance between the upper and lower radiator is equal to the effective wavelength of the lowest operational frequency. The length of each antenna radiator is equal to the half of the effective wavelength calculated for the lowest operational frequency.

The width of the feeding strip W_2 is given by [6]

$$W_2 = \frac{120\pi}{\sqrt{\varepsilon_r}} \frac{h}{Z_0} \qquad (7)$$

where h is the height of the microwave substrate, ε_r is the dielectric constant of the substrate, and the characteristic impedance of the feeding strip is required to be $Z_0 = 50\ \Omega$.
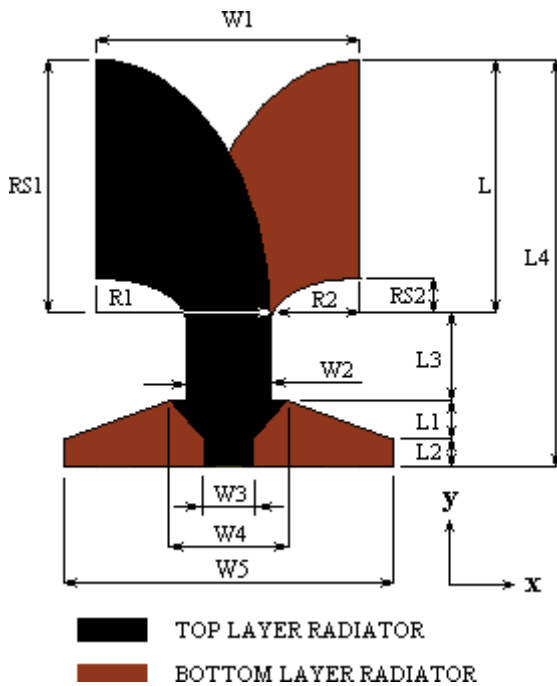

Fig. 2. Vivaldi antenna geometry.

Next, a transition from the symmetrical arms of the Vivaldi antenna to the asymmetric coaxial connector has to be designed (see Fig. 2). The transition from the balanced twin-line to a coaxial unbalanced feed point is implemented using a linear microstrip taper. The unbalanced end of the tapered balun resembles a microstrip line of width W_3 ($Z_0 = 50\ \Omega$) over a finite ground plane of width W_5. In order to approximate an ideal microstrip line, the ground plane must be much wider than the metallic strip. In the proposed design, a ratio $W_5/W_3 = 7$ is assumed [8]. The width W_4 depends on the opening angle of the strip, which is equal to $\alpha = 6°$ [8]. The length $L_1 = 0.182\ \lambda_g$ and the

length $L_3 = 0.36\ \lambda_g$ where, λ_g is the wavelength on the microwave substrate given by (11).

Numerical values of the antenna dimensions are summarized in Tab. 1.

W_1	10.140 mm
W_2	3.240 mm
W_3	1.816 mm
W_4	4.490 mm
W_5	12.712 mm
L	10.140 mm
L_1	1.511 mm
L_2	0.900 mm
L_3	2.987 mm
L_4	15.538 mm
R_1	6.690 mm
R_2	3.450 mm
R_{S1}	10.140 mm
R_{S2}	1.725 mm

Tab. 1. Numerical values of Vivaldi antenna dimensions for $f \approx 20$ GHz.

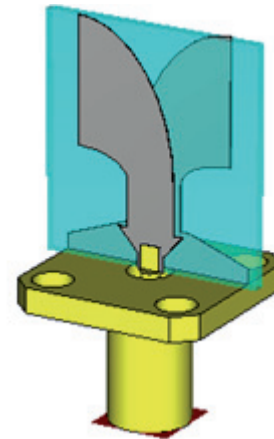The antenna was designed for the band of operational frequencies $f_1 = 20$ GHz to $f_2 = 40$ GHz.

Fig. 3. CST model of Vivaldi antenna.

A numerical model of the Vivaldi antenna connected to a 2.92 mm connector (Fig. 3) was simulated in CST Microwave Studio using transient solver.

In Fig. 4, computed and measured frequency responses of the return loss at the antenna input are compared. The bandwidth was reduced due to losses and parasitic properties of the 2.92 mm connector.
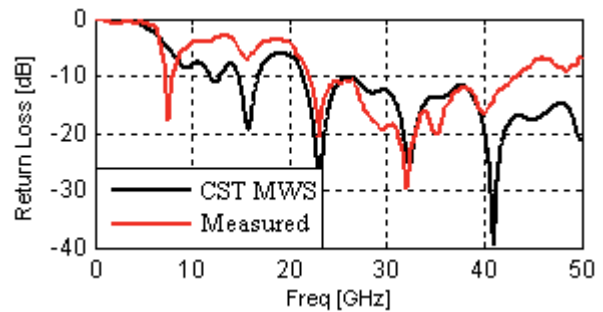

Fig. 4. Frequency response of the return loss of the Vivaldi antenna: CST MWS (black), measured (red).

The bandwidth defined by the –10 dB decrease of the return loss at the input of the measured antenna is $B = 22.43$ GHz. The real and imaginary components of the input impedance are shown in Fig. 5.
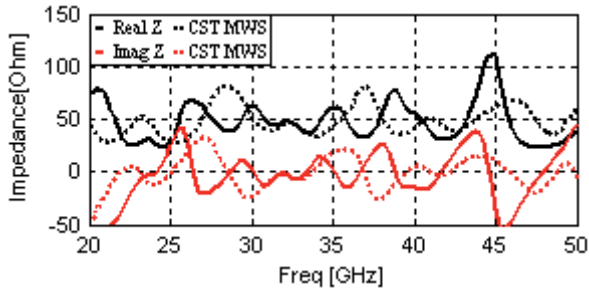

Fig. 5. Measured and simulated input impedance of the Vivaldi antenna: input resistance (black), and input reactance (red).

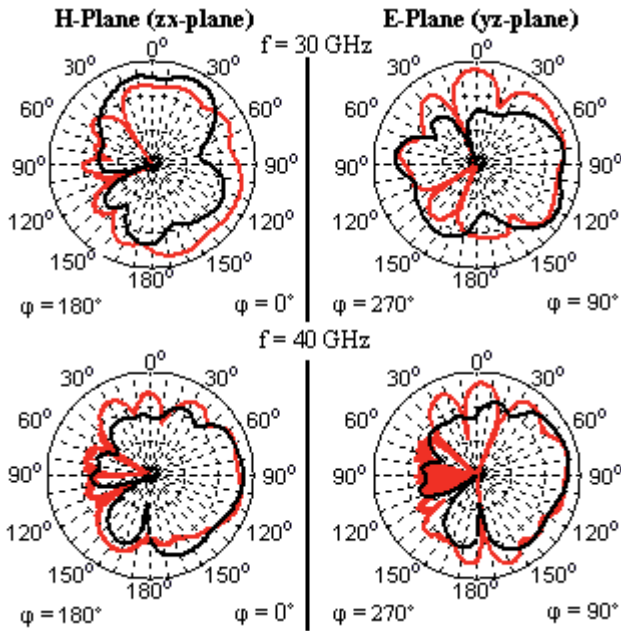Measured and computed directivity patterns are depicted in Fig. 6.

Fig. 6. Directivity patterns of the Vivaldi antenna: CST MWS (black), and measured (red).

3. Bow-Tie Antenna

The bow-tie dipole (Fig. 7) can be simply constructed and can provide good wideband parameters. The investigated antenna was designed for the microwave substrate Arlon 25N.

The resonant frequency on a microwave substrate with dielectric constant ε_r can be computed by [2]

$$f_r = \frac{2c\sqrt{m^2 + mn + n^2}}{3l\sqrt{\varepsilon_r}} \qquad (8)$$

where c is the light velocity, numbers m and n determine the operational mode of the antenna, and l is the length of the antenna arm. The length of the antenna arm can be computed using [2]

$$l = \frac{2c}{2f_r\sqrt{\varepsilon_r}} . \qquad (9)$$

Consequently, the value of the arm length l has to be modified in order to obtain its effective value [2]

$$l_{eff} = l + \frac{h}{\sqrt{\varepsilon_r}} . \qquad (10)$$

Here, h is the height of the microwave substrate.

Antenna wavelength is defined by [2]

$$\lambda_g = \frac{\lambda_0}{\sqrt{\varepsilon_{eff}}} \quad \text{where} \quad \varepsilon_{eff} = \frac{\varepsilon_r + 1}{2} + \frac{\varepsilon_r - 1}{4\sqrt{1 + \frac{12h}{l}}} . \qquad (11)$$

Here, ε_{eff} is the effective permittivity of the microwave substrate and λ_0 is the free space wavelength.
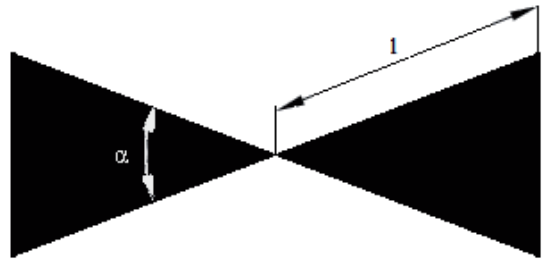

Fig. 7. Simplified geometry of the bow-tie antenna.

The opening angle α (Fig. 7) can be chosen almost in any range (10° to 80°). The angle significantly impacts parameters of the broadband antenna.

A detailed layout of the bow-tie antenna is depicted in Fig. 8. Numerical values of antenna dimensions are summarized in Tab. 2.

The antenna was designed for the band with central frequency $f_1 = 30$ GHz. The widths W_1, W_2 and lengths L_1, L_2 are dimensions of the quarter-wave transformer. The width W_5 is determined by (10) and the known angle $\alpha = 51°$.
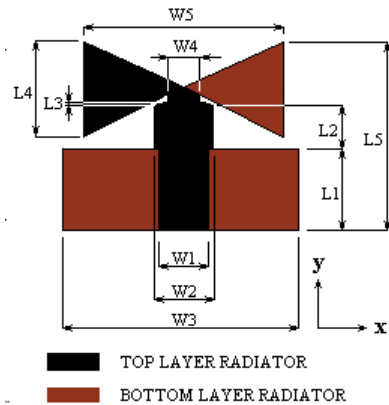

Fig. 8. Detailed geometry of the bow-tie antenna.

W_1	2.128 mm
W_2	2.531 mm
W_3	10.300 mm
W_4	1.362 mm
W_5	8.739 mm
L_1	3.529 mm
L_2	1.902 mm
L_3	0.156 mm
L_4	4.162 mm
L_5	8.191 mm

Tab. 2. Numerical values of the bow-tie antenna dimensions for $\alpha = 51°$.

A numerical model of the bow-tie antenna connected to a 2.92 mm connector (Fig. 9) was simulated in CST Microwave Studio using transient solver.
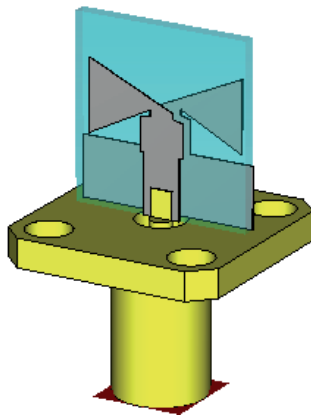

Fig. 9.   CST model of the bow-tie antenna.

Fig. 10 shows the frequency response of the computed return loss and the measured one. The bandwidth was reduced due to losses. The deviation of the measured return loss with respect to the simulated one is caused by parasitic properties of the structure (e.g., the parasitic capacity between the antenna and the attached connector). The measured antenna bandwidth is $B \geq 18.23$ GHz.
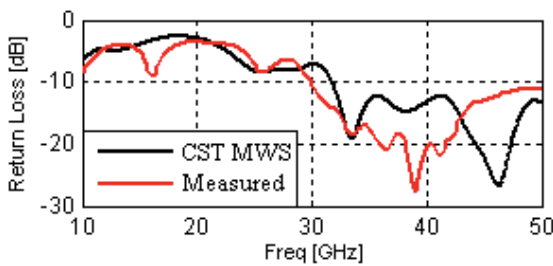

Fig. 10. Frequency response of the return loss of the bow-tie antenna: CST MWS (black), measured (red).
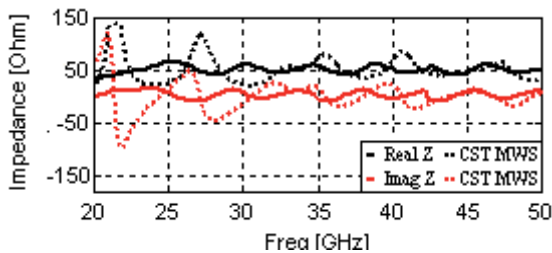

Fig. 11. Measured and simulated input impedance of the bow-tie antenna: input resistance (black), and input reactance (red).

Fig. 11 shows the measured input resistance and input reactance of the bow-tie antenna for the operational band.

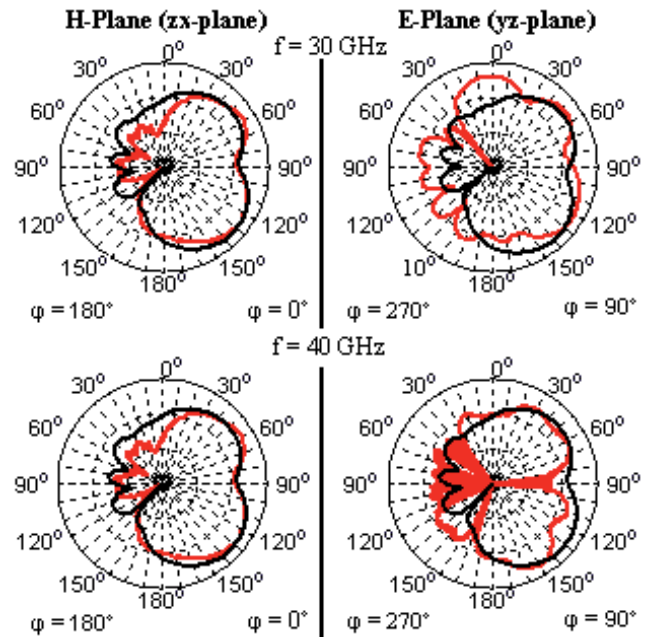Measured and computed directivity patterns of the bow-tie antenna are depicted in Fig. 12.

Fig. 12. Directivity patterns of the bow-tie antenna: CST MWS (black), and measured (red).

4.   Spiral Antenna

Dimensions of the spiral antenna are specified by the angles ψ, δ only (see Fig. 13) unlike the previous two antennas. The practical design of the spiral antenna comprises the determination of the radii R_1 and R_2. The constant R_0 can be determined from the general initial value of the angle range Φ, and the radii R_1 and R_2. The angle range Φ depends on the ratio R_2/R_1 only.
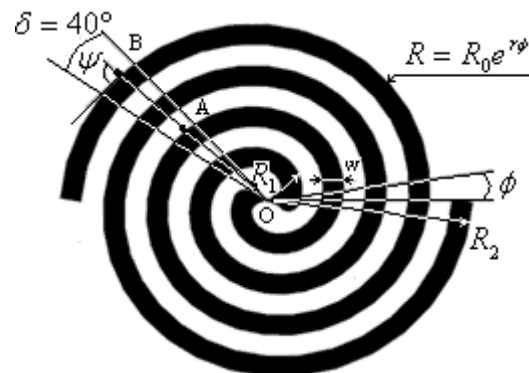

Fig. 13. Simplified geometry of the spiral antenna.

The spiral antenna is designed for a prescribed operating band $[f_2, f_1]$. The upper frequency limit f_1 determines the value of the radius $R_1 = \lambda_1/14$. The lower frequency limit f_2 is related to the parameters δ (see Fig. 13) and r (17). The antenna diameter should be slightly larger than

λ_2/π. The ratio $(R_2/R_1)/(f_1/f_2)$ is the decisive parameter for the antenna, which determines the compactness of the antenna for the desired bandwidth. The ratio is usually close to one.

The spiral antenna was designed for the microwave substrate Arlon 25N

The spiral elevation angle Ψ is given by [7]

$$\tan \psi = \frac{1}{r} \qquad (12)$$

where r is the expansion coefficient and it is related to the radius R by [7].

$$l = \frac{R}{\cos \Psi} \qquad (13)$$

where l denotes the arc length from the beginning of O. Moreover, l is finite and proportional to the radius R.

In the next step, an auxiliary quantity $\tau \leq 1$ has to be evaluated [7]

$$\tau = \exp\left[-\frac{2\pi}{|\tan\psi|} \right]. \qquad (14)$$

The quantity τ corresponds to the ratio OA/OB in Fig. 13.

The logarithmic nature of the antenna parameters can arise after converting (12) and (14) to [7]

$$r = -\frac{\log\tau}{2\pi}, \qquad (15a)$$

$$\psi = \arctan\left(\frac{2\pi}{|\log\tau|} \right). \qquad (15b)$$

The second side of the antenna strip is given by [7]

$$R = R_0 \exp[r(\psi + \delta)] \qquad (16)$$

where R_0 is a constant, r is given by (15a), Ψ is given by (15b) and the angle δ is depicted in Fig. 13.

The equation (16) is equivalent to a scaling [7]

$$K = \exp(rw). \qquad (17)$$

The dependence of the width of the spiral arm strip w on the radius R is given by [7]

$$w = R(1-K)\sin\psi. \qquad (18)$$

The second arm is obtained by rotating the first arm for 180° around the center O.

In accordance with the above equations, the spiral antenna was designed for the band of operational frequencies $f_2 = 10$ GHz to $f_1 = 50$ GHz by the following relations:

$$X_1 = 0.445 \exp(0.5645\varphi) \cos(\varphi), \qquad (19a)$$

$$Y_1 = 0.445 \exp(0.5645\varphi) \sin(\varphi), \qquad (19b)$$

$$X_2 = 0.445 \exp[0.5645(\varphi + 0.6981)] \cos(\varphi), \qquad (19c)$$

$$Y_2 = 0.445 \exp[0.5645(\varphi + 0.6981)] \sin(\varphi), \qquad (19d)$$

$$\varphi \in [0, 5.5]\,\text{rad}. \qquad (19e)$$

A wideband balun, which is connected to the antenna, serves as a transition from an asymmetric microwave connector to the symmetric input of the spiral antenna. Moreover, the balun plays the role of the impedance transformer: the impedance of the microwave connector Z_{in} = 50 Ω is converted to the input impedance of the spiral antenna Z_{ant} = 145 Ω.

The wideband transition is composed from a set of quarter-wavelength transformers of characteristic impedance

$$Z = \sqrt{Z_1 Z_2}, \qquad (20)$$

where Z_1 and Z_2 are impedances at the input and the output of the transformer.

The set of quarter-wavelength transformers is followed by a Klopfenstein tapered ground plane [9] ensuring the transition from the unbalanced line to the balanced one. The whole wideband impedance transformer (Fig. 14) is designed as a planar structure [10]. The 2.92mm connector is connected to the balun.
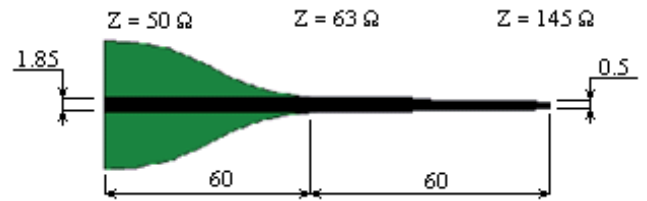

Fig. 14. The geometry of the planar impedance transformer from 50 Ω to 145 Ω.

The numerical model of the spiral antenna was created in CST Microwaves Studio. The model is shown in Fig. 15.
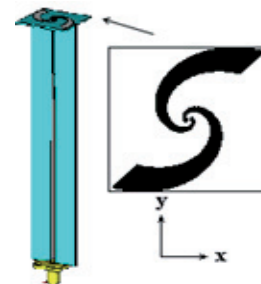

Fig. 15. CST model of the spiral antenna.

Fig. 16 shows frequency response of the return loss at the input of the spiral antenna. Measured data are depicted in red, and computed ones in black. The bandwidth was reduced due to losses. The measured data were deformed by parasitic phenomena like parasitic capacity between the antenna and the attached connector. The antenna bandwidth is $B = 25.49$ GHz. The rotate arm antenna has a major impact on the basic parameters of the antenna.
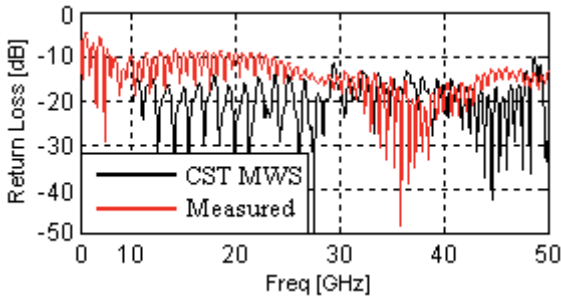
Fig. 16. Frequency response of the return loss of the spiral antenna: CST MWS (black), measured (red).

Fig. 17 shows the measured input resistance and input reactance of the spiral antenna for the operational band.
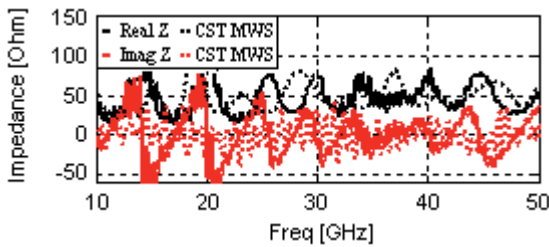

Fig. 17. Measured and simulated input impedance of the spiral antenna: input resistance (black), and input reactance (red).

Measured and computed directivity patterns of the spiral antenna at the frequency $f_2 = 40$ GHz are depicted in Fig.18 both for the H plane (left) and for the E plane (right).
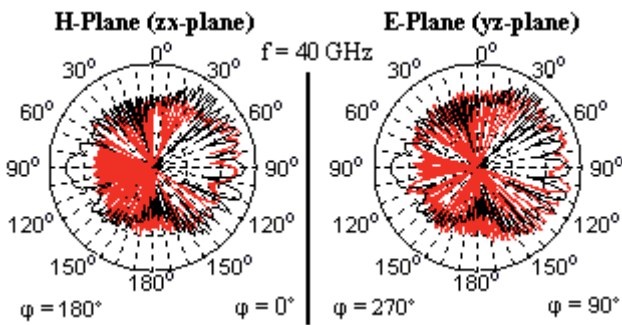

Fig. 18. Directivity patterns of the spiral antenna: CST MWS (black), and measured (red).

5. Conclusions

The paper describes the design and experimental verification of parameters of three types of wideband antennas. The bandwidth, the input impedance and directivity patterns are mutually compared in Tab. 3, 4.

Antenna	Bandwidth
Bow-Tie antenna	18.23 GHz
Vivaldi antenna	22.43 GHz
Spiral antenna	25.49 GHz

Tab. 3. Bandwidth of the investigated antennas.

The best results in terms of the bandwidth are reached by the spiral antenna. On the other hand, the structure of the spiral antenna is very complex, and the antenna has to be completed by an absorption cavity for the proper functioning. The design sensitivity related to the manufacturing precision is not critical, but this is not true when speaking about the feed strip and the balun.

The bow-tie antenna exhibits the smallest bandwidth. The structure of the bow-tie antenna is simple compared to a spiral antenna. The design sensitivity to the accuracy of the production of the bow-tie antenna is of a very fundamental nature.

The Vivaldi antenna exhibits the medium bandwidth. The design is very simple and easily tunable. The design sensitivity to the manufacturing precision is not critical, because the principle of operation is different.

Antenna	Gain@40 GHz
Bow-Tie antenna	6.32 dBi
Vivaldi antenna	5.89 dBi
Spiral antenna	7.62 dBi

Tab. 4. Gain of the investigated antennas.

The above given discussion shows that the Vivaldi antenna is the most suitable antenna for millimeter-wave applications. The Vivaldi antenna exhibits the best performance with the reference to the required characteristics.

In Fig. 19 to 21, the manufactured antenna prototypes are shown. The prototype of antennas was connected to the ground plane through the K-connector. The attached screws had a small impact in directivity patterns.
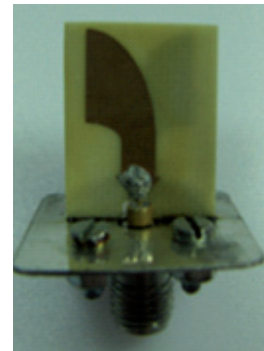

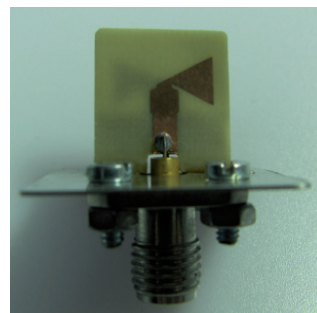**Fig. 19.** Prototype of the Vivaldi antenna.

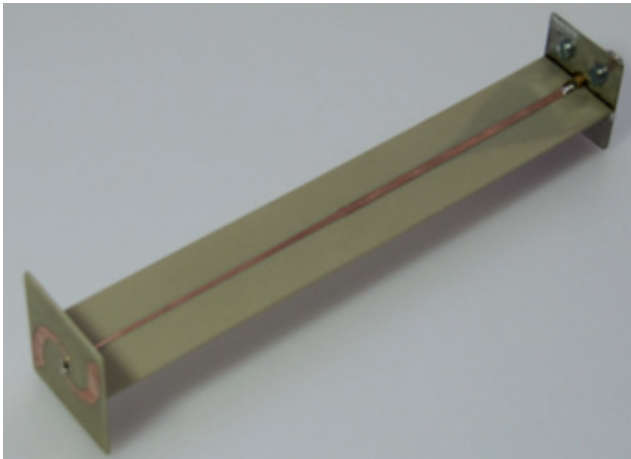**Fig. 20.** Prototype of the bow-tie antenna.

Fig. 21. Prototype of the spiral antenna.

The application of the Vivaldi antenna and bow-tie antenna was published in [11].

Acknowledgements

References

[1] PÍTRA, K. *Antennas for Millimetre-Wave Band*. Master's thesis, Brno: Brno University of Technology, 2010.

[2] RAHIM, M. K. A., ABDUK AZIZ, M. Z. A., GOH, C. S. Bow-tie microstrip antenna design. In *13th IEE International Conference on Networks Jointly held with the 2005 7th IEEE Malaysia International Conference on Communication*s, 2005, p. 17 – 20.

[3] MUKHERJEE, P., GUPTA, B. Terahertz (THz) frequency sources and antennas - a brief overview. *International Journal on Infrared and Millimetre Waves*, 2008, vol. 29, no. 12, p. 1091 – 1102.

[4] POULARIKAS, A. *Antenna Handbook of Antennas in Wireless Communications*. Godara: CRC Press, 2002, p 30 – 40.

[5] HUDLIČKA, M. *Coplanar Antenna with Leaky Wave*. Master's thesis. Prague: Czech Technical University in Prague, 2004.

[6] ABBOSH, A. Directive antenna for ultra-wideband medical imaging systems. *International Journal on Antennas and Propagation*, 2008, vol. 2008, Article ID 854012.

[7] PROCHÁZKA, M. *Antennas – Handbook.* Prague: BEN Publishing, 2005, p. 67 – 69 (in Czech).

[8] VASILIADIS, T. G., VAITSOPOULOS, E. G., SERGIADIS, G.D. A wideband printed dipole antenna with optimized tapered feeding balun for ISM and FWA bands. *Microwave and Optical Technology Letters*, 2004, vol. 43, no. 5, p. 437 – 441.

[9] KLOPFENSTEIN, R. W. A transmission line taper of improved design. *Proceedings of the IRE*, 1956, vol. 44, p. 31 – 35.

[10] NGUYEN, C. *Analysis Methods for RF, Microwave, and Millimeter-Wave Planar Transmission Line Structures*. John Wiley and Sons, 2000, p. 63 – 81.

[11] PÍTRA, K., RAIDA, Z. Wideband feeders for millimeter-wave horn antennas. In *Proceedings of the 15th Conference on Microwave Techniques, COMITE*. Brno (Czech Republic), 2010, p. 39 – 41.

About Authors

Kamil PÍTRA was born in Strakonice, Czech Republic in April 1984. He graduated at the Faculty of Electrical Engineering a Communication (FEEC), Brno University of Technology (BUT), in 2010. He is currently a Ph.D. student at the Dept. of Radio Electronics, BUT.

Zbyněk RAIDA received Ing. (M.Sc.) and Dr. (Ph.D.) degrees from the Brno University of Technology (BUT) in 1991 and 1994, respectively. Since 1993, he has been with the Department of Radio Electronics, Brno University of Technology as the assistant professor (1993 to 1998), associate professor (1999 to 2003), and full professor (since 2004). From 1996 to 1997, he spent 6 months at the Laboratoire de Hyperfrequences, Universite Catholique de Louvain, Belgium as an independent researcher.

Prof. Raida has authored or coauthored more than 90 papers in scientific journals and conference proceedings. His research has been focused on numerical modeling and optimization of electromagnetic structures, application of neural networks to modeling and design of microwave structures, and on adaptive antennas.

Prof. Raida is a member of the IEEE Microwave Theory and Techniques Society. From 2001 to 2003, he chaired the MTT/AP/ED joint section of the Czech-Slovak chapter of IEEE. In 2003, he became the Senior Member of IEEE. From 2001 to 2010, Prof. Raida was an editor-in-chief of the Radioengineering Journal.